International Forum on Aeroelasticity and Structural Dynamics
IFASD 2026
16-18 June 2026, Goettingen (GERMANY)

REGIONAL AIRCRAFT WING ASSESSMENT OF ACTIVE GUST LOAD ALLEVIATION TECHNOLOGIES FOR HIGH ASPECT RATIO ULTRA EFFICIENT REGIONAL AIRCRAFT WING

*Giovanni Marco CAROSSA**[1], *Andrea DE MEDA*[1] , *Elena RONCOLINI*[1] , *Francesco TOFFOL*[1] , *Sergio RICCI*[1]

[1] Department of Aerospace Science and Technology, Politecnico di Milano, Via la Masa 34, 20156, Milano, Italy.

Keywords: Active Gust Load Alleviation, High-Aspect-Ratio Wings,

Aeroelastic Modelling, Unsteady Aerodynamics, Closed-Loop Control, Scaled Wind-Tunnel Testing

Abstract:

High-aspect-ratio wings are a key enabler for improving the aerodynamic efficiency of next-generation regional aircraft, but their inherent structural flexibility leads to increased sensitivity to gust and manoeuvre loads. This paper presents a comprehensive numerical framework for the assessment of active load alleviation technologies applied to a high-aspect-ratio regional wing representative of an ultra-efficient regional aircraft (UERA) with aspect ratio 16. A linear time-invariant aeroelastic model is developed within the NeoCASS environment, combining steady and unsteady aerodynamic methods and multiple mass configurations compliant with CS-25 requirements. The model is formulated in state-space representation and integrated into a modular aero-servo-elastic virtual simulator implemented in Simulink, enabling time-domain simulations and control law development. Gust Load Alleviation (GLA) strategies based on Static Output Feedback (SOF) and Linear Quadratic Gaussian (LQG) control architectures are designed and optimized, accounting for aero-servo-elastic performance, robustness, and actuator constraints. Closed-loop simulations demonstrate significant reductions in wing root bending moment, exceeding 20% under discrete gust excitation. In addition, Manoeuvre Load Alleviation (MLA) strategies based on symmetric aileron and load control tab deflections are investigated, showing effective load redistribution during manoeuvres. To support experimental validation, a 1:6 scale aeroelastic model equipped with active control surfaces and a gust generation system is under development for wind tunnel testing, targeting Technology Readiness Level 5. The results highlight the fundamental role of active control in enabling lightweight, high-aspect-ratio wing designs while meeting certification requirements.

1 INTRODUCTION

Active gust and maneuver load alleviation technologies are essential enablers for achieving significant structural weight reductions in very high–aspect-ratio (HAR) wings, such as AR16 configuration, by mitigating the increased sensitivity to aeroelastic loads that naturally accompanies slender, flexible lifting surfaces.

High-aspect-ratio wings offer clear aerodynamic advantages—most notably improved lift-to-drag ratio and reduced fuel burn—but their greater span and reduced structural stiffness make them inherently more vulnerable to gust-and maneuver-induced load excursions. Without dedicated alleviation strategies, these load peaks drive conservative structural sizing, leading to heavier spars, ribs, and skins. Modern research shows that active load control enables the use of high-aspect-ratio wings while maintaining relatively low structural weight, directly counteracting the penalties associated with increased flexibility.

In this context load alleviation systems—implemented through coordinated actuation of ailerons, spoilers, tabs, or variable-camber surfaces—play a pivotal role in shaping the dynamic response of the wing. By reducing wing-root bending moments and smoothing transient load distributions, these technologies allow designers to relax structural margins, enabling lighter primary structures without compromising safety or certification requirements. Recent studies highlight how advanced control strategies, including variable-camber concepts, can effectively reduce gust loads and improve ride quality, supporting the design goals of modern civil aircraft with increasingly slender wings.

For regional transport aircraft adopting AR16 wings, the integration of such active alleviation functions is therefore not merely beneficial but fundamental: it unlocks the aerodynamic potential of the configuration while ensuring compliance with CS-25 load criteria, ultimately contributing to lower operating costs, reduced emissions, and improved overall performance.

Wind tunnel aero-servo-elastic experiments play a fundamental role in the demonstration and validation of active control technologies for load alleviation. They are essential to experimentally assess the performance, robustness, and stability of Gust Load Alleviation (GLA) control laws under representative operating conditions. Beyond technology demonstration, wind tunnel testing provides a controlled laboratory environment to validate numerical aeroelastic prediction tools, reducing modelling uncertainties and increasing confidence in simulation-based design methodologies. Within this framework, experimental validation at model scale is a key step to advance the maturity of active control solutions toward Technology Readiness Level 5 (TRL 5). According to the NASA definition, TRL 5 corresponds to “component and/or breadboard validation in a relevant environment,” meaning that the technology is validated through testing under conditions that are representative of the intended operational environment, though not yet at full scale.

2 REFERENCE AIRCRAFT AND AEROELASTIC MODEL

Hybrid- Electric Regional Architecture (HERA), a Clean Aviation project [2], for present work was in charge to provide high level requirements and the aerodynamic configuration shapes (CAD) of UERA (Ultra Efficient Regional Aircraft) configuration and aerodynamic geometry to be analyzed here (Figure 1). Unlikely additional structural and aero-servo-elastic data are required

for loads alleviation controller development and aeroelastic wind-tunnel model scaling. This fundamental design information was developed by Clean Aviation project HERWINGT [1]. A dedicated trade-off study evaluated the impact of increasing wing aspect ratio up to 16, including structural sizing, load-alleviation benefits, and structural dynamics behavior.

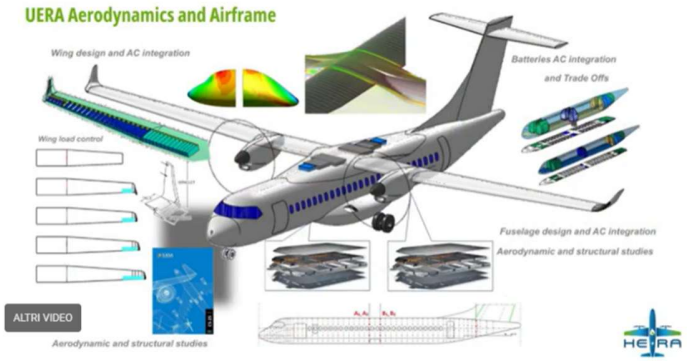


Figure 1: Clean Aviation HERA&HERWINGT Regional Aircraft (UERA) transport aircraft

The outer wing extension is equipped with a dedicated load control tab (LC tab), which is not devoted to the aircraft handling, but only to load alleviation purposes.

2.1 Aeroelastic Modelling Approach:

In the light of this, aircraft structural preliminary sizing was carried out using NeoCASS [3][4][5], a MATLAB-based aeroelastic conceptual design tool. NeoCASS provides a fully stressed structural layout in which the lifting surfaces and supporting elements are represented by an equivalent beam-based A/C structural model. This formulation enables efficient structural sizing while maintaining sufficient fidelity for subsequent dynamic and control analyses.

On the aerodynamic side, the model relies on a combination of Vortex Lattice Method (VLM) for steady aerodynamics and Doublet Lattice Method (DLM) for unsteady aerodynamic effects. This hybrid approach ensures an accurate representation of both the static load distribution and the frequency-dependent aeroelastic response, which is essential for the development and validation of gust load-alleviation control laws.

Structural sizing of A/C configuration considered 35 CS-25/EASA-25 maneuvers across four mass configurations - (MTOW, MLW, MZF, OEW).

Table 1 - Mass configurations used for sizing

Mass configuration	Fuel	Payload
MTOW	100%	100%
MLW	80%	100%
MZFW	0%	100%
OEW	0%	0%

These mass configurations ensure adequate coverage of the structural load cases throughout the operational envelope, providing a robust foundation for the aeroelastic model later integrated into the time-domain simulation environment.

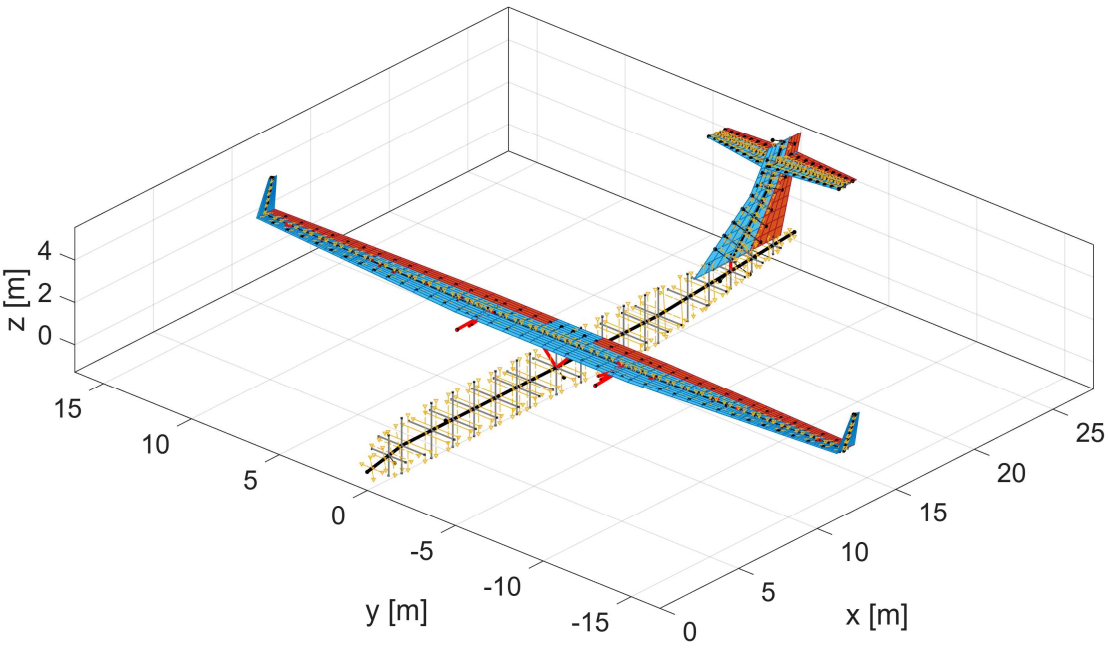
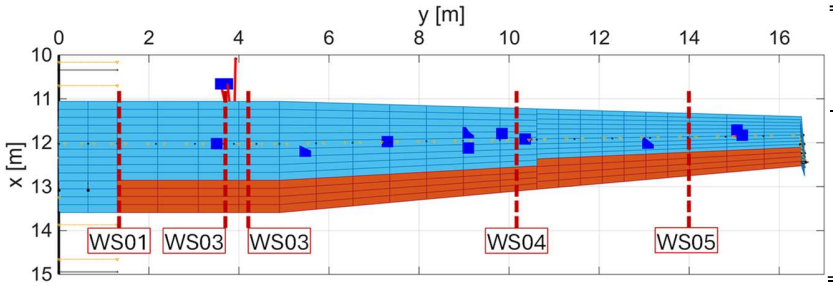


Figure 2: 3D Views of the UERA aeroelastic stick model realized with NeoCASS

The resulting A/C level aeroelastic model (Figure 2) served as numerical model for the investigation of the active control technologies.

Key point for following analysis of GLA system is the loads monitoring definition. Figure 3 shows the five wing spanwise loads monitoring stations for internal forces monitoring. GLA controller is based on the feedback of structural responses, i.e. accelerations, measured with a set of accelerometers (blue points).



Load Monitoring Station	Description
WS01	Wing root
WS02	Inner engine
WS03	Outer engine
WS04	Inner aileron
WS05	Inner tab

Figure 3: Wing spanwise structural loads monitoring stations and accelerometers locations

2.2 State Space Modelling

The present chapter describes the formulation of the state–space (SS) model of the aeroelastic stick model developed within the HERWINGT project [1]. The formulation builds directly on the finite element structural model presented in the previous chapter and aims at providing a continuous-time linear time-invariant (LTI) representation suitable for time-domain simulations, aeroelastic stability analysis, and subsequent control law development.

Once the finite element model is projected onto a reduced modal basis, the modelling of the elasto-mechanical system becomes straightforward. The structural equations of motion are expressed in modal coordinates, where the generalized mass, damping, and stiffness matrices are readily available from the modal analysis. Under the assumption of linear structural behavior and small perturbations about the trimmed condition, the resulting structural model is linear and time invariant. The state vector is defined in terms of the modal generalized displacements and their corresponding velocities, leading to a standard first-order SS formulation of the elastic dynamics.

The main modelling challenge lies in the representation of the unsteady aerodynamic forces and their integration into a continuous SS framework. The aerodynamic loads are expressed in terms of Generalized Aerodynamic Forces (GAFs), which account for the effects of structural motion, atmospheric gust excitation, and control surface deflections. These forces are computed in the frequency domain using the Doublet Lattice Method (DLM), which provides the aerodynamic influence coefficients at a discrete set of reduced frequencies, k.

$$\boldsymbol{GAFs} = q_\infty(\boldsymbol{H_{am}}(k, Ma)\boldsymbol{q} + \boldsymbol{H_{ag}}(k, Ma)v_g \tag{1}$$

Since the DLM delivers frequency-dependent aerodynamic forces, a direct time-domain implementation is not possible. To overcome this limitation, an identification procedure is required to approximate the frequency-domain aerodynamic behavior with an equivalent time-domain representation. This task is performed using a Rational Function Approximation (RFA) technique, which enables the transformation of the discrete-frequency GAFs into a continuous LTI model by introducing a set of aerodynamic lag states.

$$\mathbf{H}_{am}(p) \approx \mathbf{D^0}_a + p\mathbf{D^1}_a + p^2\mathbf{D^2}_a + \mathbf{C}_a(p\mathbf{I} - \mathbf{A}_a)^{-1}\left(\mathbf{B^0}_a + p\mathbf{B^1}_a + p^2\mathbf{B^2}_a\right) \tag{2}$$

The RFA identification procedure is embedded in the NeoCASS framework [3][4][5]. For each relevant combination of flight condition and mass configuration, the DLM-based GAFs are approximated by rational functions of the Laplace variable, whose coefficients are identified to best fit the aerodynamic response over the selected reduced-frequency range. The resulting aerodynamic lag states capture the essential unsteady aerodynamic effects associated with circulation buildup and wake dynamics, while preserving a state-space structure compatible with time-domain analysis.

$$\begin{cases} \dfrac{d\mathbf{x}_a}{dt} &= \dfrac{1}{t_a}\mathbf{A}_a\mathbf{x}_a + \dfrac{1}{t_a}\mathbf{B^0}_a\mathbf{q} + \mathbf{B^1}_a\dot{\mathbf{q}} + t_a\mathbf{B^2}_a\ddot{\mathbf{q}} \\ \mathbf{Q_a} &= \mathbf{C}_a\mathbf{x}_a + \mathbf{D^0}_a\mathbf{q} + t_a\mathbf{D^1}_a\dot{\mathbf{q}} + t_a^2\mathbf{D^2}_a\ddot{\mathbf{q}} \end{cases} \rightarrow \begin{cases} \dot{\mathbf{x}}_a &= \mathbf{A}\mathbf{x_a} + \mathbf{B}\mathbf{q} \\ \boldsymbol{Q_a} &= \mathbf{C}\mathbf{x_a} + \mathbf{D}\mathbf{q} \end{cases} \tag{3}$$

Once the aerodynamic lag states are identified, the aerodynamic SS model is coupled with the structural SS model to obtain the complete aeroelastic representation. The coupling is performed through the generalized modal coordinates, ensuring a consistent exchange of forces and motions between the structural and aerodynamic subsystems. The resulting model represents the aircraft aero-servo-elastic behavior in a unified SS framework, including elastic dynamics, unsteady aerodynamics, gust excitation, and control surface effects.

$$\begin{bmatrix} \mathbf{I} & \mathbf{0} & \mathbf{0} \\ \mathbf{0} & \mathbf{M_{hh}} - q_\infty t_a^2 \mathbf{D^2}_a & \mathbf{0} \\ \mathbf{0} & -t_a^2 \mathbf{B^2}_a & t_a \mathbf{I} \end{bmatrix} \frac{d}{dt} \begin{bmatrix} \mathbf{q} \\ \dot{\mathbf{q}} \\ \mathbf{x}_a \end{bmatrix} =$$

$$+ \begin{bmatrix} \mathbf{0} & \mathbf{I} & \mathbf{0} \\ -\left(\mathbf{K_{hh}} - q_\infty \mathbf{D^0}_a\right) & -\left(\mathbf{C_{hh}} - q_\infty t_a \mathbf{D^1}_a\right) & q_\infty \mathbf{C}_{a+g} \\ \mathbf{B^0}_a & t_a \mathbf{B^1}_a & \mathbf{A}_{a+g} \end{bmatrix} \begin{bmatrix} \mathbf{q} \\ \dot{\mathbf{q}} \\ \mathbf{x}_{a+g} \end{bmatrix}$$

$$+ \frac{1}{V_\infty} \begin{bmatrix} \mathbf{0} & \mathbf{0} & \mathbf{0} \\ q_\infty \mathbf{D^0}_{ag} & q_\infty t_a \mathbf{D^1}_{ag} & q_\infty t_a^2 \mathbf{D^2}_{ag} \\ \mathbf{B^0}_{ag} & t_a \mathbf{B^1}_{ag} & t_a^2 \mathbf{B^2}_{ag} \end{bmatrix} \begin{bmatrix} \mathrm{v}_g \\ \dot{v}_g \\ \ddot{v}_g \end{bmatrix} \tag{4}$$

$$+ \begin{bmatrix} \mathbf{0} & \mathbf{0} & \mathbf{0} \\ q_\infty \mathbf{D^0}_{ac} & q_\infty t_a \mathbf{D^1}_{ac} & q_\infty t_a^2 \mathbf{D^2}_{ac} \\ \mathbf{B^0}_{ac} & t_a \mathbf{B^1}_{ac} & t_a^2 \mathbf{B^2}_{ac} \end{bmatrix} \begin{bmatrix} \delta_c \\ \dot{\delta}_c \\ \ddot{\delta}_c \end{bmatrix}$$

Which can be re-written in the compact for of:

$$\begin{cases} \dot{\boldsymbol{x}}_{\boldsymbol{ae}} = \boldsymbol{A}\boldsymbol{x}_{\boldsymbol{ae}} + \boldsymbol{B}_{\boldsymbol{g}}\boldsymbol{u}_{\boldsymbol{g}} + \boldsymbol{B}_{\boldsymbol{c}}\boldsymbol{u}_{\boldsymbol{c}} \\ \boldsymbol{y} = \boldsymbol{C}\boldsymbol{x}_{\boldsymbol{ae}} + \boldsymbol{D}_{\boldsymbol{g}}\boldsymbol{u}_{\boldsymbol{g}} + \boldsymbol{D}_{\boldsymbol{c}}\boldsymbol{u}_{\boldsymbol{c}} \end{cases} \tag{5}$$

To comply with the requirements of the RFA formulation, dedicated input filters are introduced to generate time derivatives of the input signals up to second order. These filters are applied to gust and control surface inputs, ensuring compatibility with the aerodynamic state equations and maintaining the overall LTI structure of the model.

$$\begin{bmatrix} \dot{\boldsymbol{x}} \\ \ddot{\boldsymbol{x}} \end{bmatrix} = \begin{bmatrix} \mathbf{0} & \mathbf{1} \\ -\boldsymbol{\omega}_\mathbf{0}^\mathbf{2} & -\mathbf{2}\boldsymbol{\xi}\boldsymbol{\omega}_\mathbf{0} \end{bmatrix} \begin{bmatrix} \boldsymbol{x} \\ \dot{\boldsymbol{x}} \end{bmatrix} + \begin{bmatrix} \mathbf{0} \\ -\boldsymbol{\omega}_\mathbf{0}^\mathbf{2} \end{bmatrix} \boldsymbol{\delta}_{\boldsymbol{cmd}}$$

$$\begin{bmatrix} \boldsymbol{\delta}_{\boldsymbol{c}} \\ \dot{\boldsymbol{\delta}}_{\boldsymbol{c}} \\ \ddot{\boldsymbol{\delta}}_{\boldsymbol{c}} \end{bmatrix} = \begin{bmatrix} \mathbf{1} & \mathbf{0} \\ \mathbf{0} & \mathbf{1} \\ -\boldsymbol{\omega}_\mathbf{0}^\mathbf{2} & -\mathbf{2}\boldsymbol{\xi}\boldsymbol{\omega}_\mathbf{0} \end{bmatrix} \begin{bmatrix} \boldsymbol{x} \\ \dot{\boldsymbol{x}} \end{bmatrix} + \begin{bmatrix} \mathbf{0} \\ \mathbf{0} \\ -\boldsymbol{\omega}_\mathbf{0}^\mathbf{2} \end{bmatrix} \boldsymbol{\delta}_{\boldsymbol{cmd}} \tag{6}$$

Therefore, the final aero-elastic system becomes:

$$\begin{cases} \dot{\boldsymbol{x}}_{\boldsymbol{ae}} = \boldsymbol{A}\boldsymbol{x}_{\boldsymbol{ae}} + \boldsymbol{B}_{\boldsymbol{g}}\boldsymbol{u}_{\boldsymbol{g}} + \boldsymbol{B}_{\boldsymbol{c}}\boldsymbol{\delta}_{\boldsymbol{cmd}} \\ \boldsymbol{y} = \boldsymbol{C}\boldsymbol{x}_{\boldsymbol{ae}} + \boldsymbol{D}_{\boldsymbol{g}}\boldsymbol{u}_{\boldsymbol{g}} + \boldsymbol{D}_{\boldsymbol{c}}\boldsymbol{\delta}_{\boldsymbol{cmd}} \end{cases} \tag{7}$$

Several SS models have been identified to cover the range of flight conditions and mass configurations of interest for the project. Each model is associated with a specific operating point and aerodynamic database, allowing systematic parametric studies and robustness assessments.

At this stage, actuator dynamics are not explicitly included in the SS formulation. Their effect will be accounted for at a later stage through appropriate shaping filters applied to the control surface command signals. This modelling choice allows the present chapter to focus on the core aeroelastic coupling, while preserving flexibility for future extensions of the aero-servo-elastic model.

3 MANOEUVRE LOAD ALLEVIATION

Manouvre Load Alleviation (MLA) is a “well known” methodology, used to redistribute the aerodynamic load. This reduces the internal forces and the sizing load. This paragraph describes how the MLA is performed on the UERA model.

The wing control surfaces (namely: ailerons and load control tabs) are deflected to push the aerodynamic load distribution more inboard, reducing the bending moment for the inner part of the wing, as sketched in Figure 4. In this work, the control surfaces are deflected symmetrically.

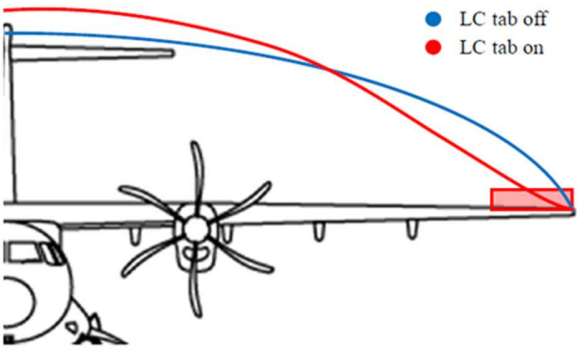


Figure 4: Working principle of load alleviation

To investigate the potential of control surfaces in reducing loads for MLA, the most severe trim condition for the aircraft was searched, and it resulted to be a 2.5g pull-up manoeuvre at V_C.

The control law for the surface deflection is proportional to the load factor variation, Δn, w.r.t. the 1g trim condition:

$$\delta = k\Delta n \tag{8}$$

Such law is designed to act statically; hence it is fully decoupled from the GLA controller. This is implemented by the usage of low frequency low-pass filters, which decouples rigid body dynamic from the elastic response of the wing.

Symmetric, incremental deflections of the LC tabs and ailerons were applied, with angles of -5◦, -10◦, -15◦, and -20◦ in case of positive load factor conditions (up wise lift).

Table 2: different values of gain and equivalent control surface rotation for MLA

Deflection	-5°	-10°	-15°	-20°
K	-3.33	-6.67	-10.00	-13.33

Three different control surfaces combinations are investigated:

1. LC tab deflection only,

2. Aileron deflection only,

3. Coupled LC tab and aileron deflection.

Results for the open-loop condition (without MLA) for different wing -AR values are reported in Figure 5. The WRBM of the UERA AR16 configuration is 27.7% higher than that of the UERA AR12 configuration. This load increase justifies the importance of MLA in limiting the associated weight penalty caused by the increase in WRBM.

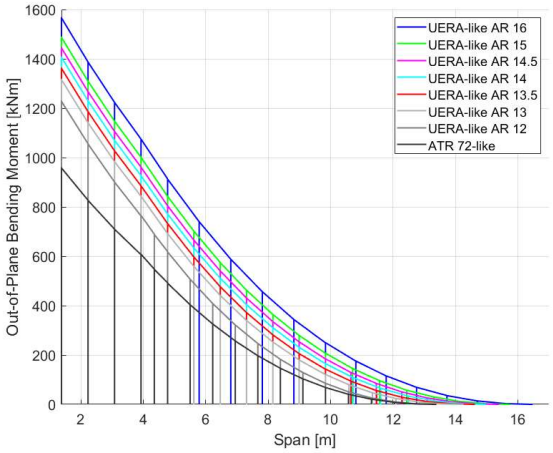


Figure 5: Out of plane bending moment evolution with the AR for the most critical manoeuvre used during sizing

A parametric analysis on the different gain values of Table 2 is performed for all the aspect ratio considered in the UERA wing trade off design, and the results are presented in Figure 6

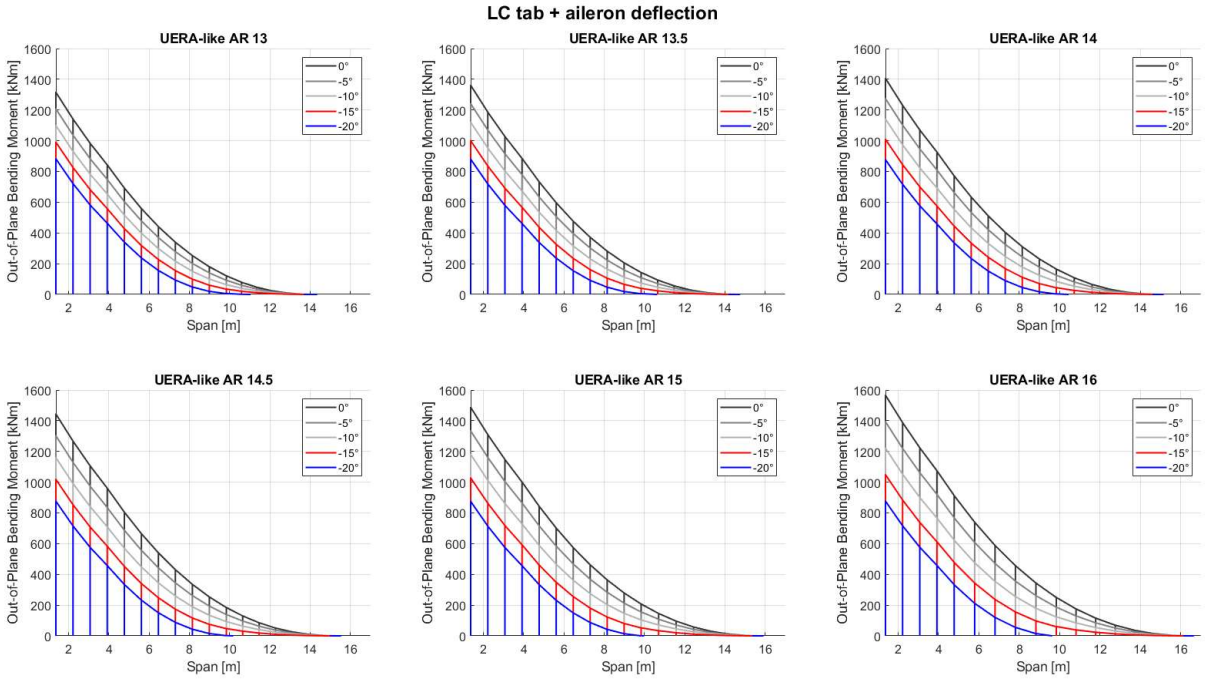


Figure 6: Effect of MLA on the bending moment for different AR

4 GUST ALLEVIATION CONTROLLERS

The purpose of this methodological framework is to justify the selection of the development of control architecture for the Gust Load Alleviation (GLA) function on a regional turboprop aircraft such as the UERA. The methodology ensures that the chosen controller satisfies aero-servo-elastic performance requirements, CS-25 compliance [6], implementation feasibility on a here assumed hybrid mechanical + EHA architecture, robustness to operational variability and structural

uncertainties. More in details, for UERA specific considerations about relevant structural characteristics can be summarized:

- Wing with soft bending mode → high gust sensitivity
- Horizontal Tail Plane with significant torsional mode → tail load sensitivity
- Mechanical + EMA hybrid controls architecture → bandwidth and saturation constraints
- Need for low-complexity GLA for certification and retrofit feasibility

The adopted methodology leads to possible layered control architecture combining LQE, LQG and SOF. This structure ensures effective gust load alleviation, compatibility with UERA structural dynamics, manageable certification effort, robustness to operational variability, and safe degraded-mode behavior. Role of each controller in the GLA chain can be assumed as follows.

4.1 Static Output Feedback Controller

The first controller developed is based on the simple Static Output Feedback (SOF) architecture [9][10], meaning that the control inputs are computed as linear combination of the measures through a gain matrix and no dynamics is involved in the controller. This is possible thanks to an a-priori integration of the acceleration to obtain the structural velocities. This leads to a gain matrix $n_{surfaces} \times n_{inputs} = 3 \times$, for a total of 111 possible variables to be defined. The number of design parameters can be drastically reduced with some physical based assumptions.

- Since only vertical gust are assumed, the aircraft response is mainly symmetric, this suggests moving the control surfaces symmetrically.
- The elevator impacts low frequencies gusts, the one interested by the rigid body motion of the aircraft. For this reason, it is reasonable to compute its feedback on quantities measured on the centre of gravity.
- The ailerons and the load control tabs are moved of the same quantity δ_{Aile}=δ_{LC}
- Further assumptions can be done to force the independent/linked right/left surfaces motion

In general, the controllers developed have range from 6 to 7 design variables (elements of the gain matrix) to be defined.

The aero-servo-elastic system is in its state-space representation and the control input is defined as a linear combination of the system measures, thus:

$$\delta_c = -Gy \tag{9}$$

that can be replaced into the canonical state-space model form, leading to the closed loop state space model:

$$\begin{cases} \dot{\boldsymbol{x}} = \left(\boldsymbol{A} - \boldsymbol{B_u}(\boldsymbol{I} + \boldsymbol{GD_u})^{-1}\boldsymbol{GC}\right)\boldsymbol{x} + (\boldsymbol{B_g} - \boldsymbol{B_u}\left(\boldsymbol{I} + \boldsymbol{GD_{yu}}\right)^{-1}\boldsymbol{GD_g})v_g \\ \boldsymbol{y} = \left(\boldsymbol{I} - \boldsymbol{D_u}(\boldsymbol{I} + \boldsymbol{GD_u})^{-1}\boldsymbol{G}\right)\boldsymbol{Cx} + \left(\boldsymbol{I} - \boldsymbol{D_u}(\boldsymbol{I} + \boldsymbol{GD_u})^{-1}\boldsymbol{G}\right)\boldsymbol{D_g}v_g \end{cases} \tag{10}$$

that in a more compact form becomes:

$$\begin{cases} \dot{\boldsymbol{x}}_{\boldsymbol{ae}} = \boldsymbol{A_{CL}}\boldsymbol{x_{ae}} + \boldsymbol{B_{CL,g}}v_g \\ \boldsymbol{y} = \boldsymbol{C_{CL}}\boldsymbol{x_{ae}} + \boldsymbol{D_{CL,g}}v_g \end{cases} \tag{11}$$

In the latest equation, the control surface input vanished since it is directly proportional to the gain matrix.

The optimization procedure set up to define the optimal gains is based on the minimization of the ratio between open loop and closed loop responses, that in the case of a GLA controller are bending and torsional moment measured in different station spanwise, but in a more general case they can be whichever output of the aero-servo-elastic system.

$$f(g) = \sum_{i=1}^{n} w_i \frac{\max\ |y_{i,CL}(t)|}{\max\ |y_{i,OL}(t)|} \tag{12}$$

The optimization is constrained and guarantees the stability of the system across the design points through the eigenvalues analysis of the closed loop state matrix, by forcing their aero-servo-elastic damping to be greater than a provided threshold.

$$\xi > 1\% \tag{13}$$

Additionally, a constraint on the performances of the actuation system is imposed, limiting the rotation rate of the control surfaces to be $\dot{\delta}_c < 100\,^{\circ}/_{S}$. This lates constraint will be further analysed and modified when the real actuator's performances will be available. However, this limit is accepted for the new generation Electro-Mechanical Actuators (EMAs).

4.2 Linear Quadratic Gaussian Regulator

The second developed controller is based on Linear Quadratic Gaussian (LQG) architecture. With respect to SOF, where a memoryless static gain is acting directly on measured outputs, LQG is a dynamic controller with its own internal states (the estimator), enabling optimal closed-loop dynamics. This is assuring much higher performance and applicability to real aircraft.

The fundamentals of optimal control theory are briefly recalled in the following, without entering the detailed mathematical formulation, which lies beyond the scope of the present work. Given the aeroelastic system in its state-space representation

$$\begin{cases} \dot{\boldsymbol{x}} = \boldsymbol{A}\boldsymbol{x} + \boldsymbol{B}\boldsymbol{u} \\ \boldsymbol{y} = \boldsymbol{C}\boldsymbol{x} + \boldsymbol{D}\boldsymbol{u} \end{cases} \tag{14}$$

A full state optimal controller is given by:

$$\boldsymbol{\delta_c} = -\boldsymbol{G}\boldsymbol{x} \tag{15}$$

The gain matrix G is determined by solving a stationarity problem associated with the optimal control formulation. The functional to be minimized is a quadratic measure of the weighted performance, z, and control, u, effort.

$$J = \int_0^{\infty} \left(\boldsymbol{z}^T \boldsymbol{Q} \boldsymbol{z} + \boldsymbol{u}^T \boldsymbol{R} \boldsymbol{u}\right) dt \tag{16}$$

Which minimization provides the Riccati's equation specialized for the optimal control case

$$\boldsymbol{A}^T\boldsymbol{P} + \boldsymbol{P}\boldsymbol{A} - \boldsymbol{P}\boldsymbol{B}\boldsymbol{R}^{-1}\boldsymbol{B}^T\boldsymbol{P} + \boldsymbol{Q} = \boldsymbol{0} \tag{17}$$

The algebraic solution provides the optimal gain matrix G as:

$$\boldsymbol{G = R^{-1}B^{T}P} \tag{18}$$

The optimization variables of the problem are the weighting matrices $\boldsymbol{Q}$ and $\boldsymbol{R}$, which define the trade-off between state regulation performance and control effort in the quadratic cost function.

In an aeroelastic system, the full state is generally not directly measurable. For this reason, here a Linear Quadratic Estimator (LQE), namely a Kalman filter, is implemented to reconstruct the complete state vector from the available measurements. The minimization of the estimation error between the actual state and the estimated one can be formulated in a manner analogous to the optimal gain matrix derivation.

In this framework, Q represents the process noise covariance matrix, accounting for uncertainties associated with the system dynamics and unmodeled disturbances, whereas R denotes the measurement noise covariance matrix, representing the uncertainty related to sensor measurements and acquisition noise.

$$\boldsymbol{A^{T}P + PA - PCR^{-1}C^{T}P + Q = 0} \tag{19}$$

And the observer gain matrix

$$\boldsymbol{L = PB^{T}R^{-1}} \tag{20}$$

The observed state becomes:

$$\begin{aligned} \boldsymbol{\dot{o}} &= \boldsymbol{Ao + Bu + L(y - Co - Du)} \\ &= \boldsymbol{\widehat{A}o + \widehat{B}u + Ly} \end{aligned} \tag{21}$$

And the controller input is defined proportionally to the observed state:

$$\boldsymbol{\delta_c = -Go} \tag{22}$$

In this work, the weight $\boldsymbol{Q}$ and $\boldsymbol{R}$ matrices associated with both the optimal LQR gain matrix $\boldsymbol{G}$ (18) and the LQE gain matrix $\boldsymbol{L}$ (20) are obtained with an optimization procedure.

4.2.1 Linear Quadratic Regulator (LQR): Optimization

Being the cost function in a max(f) form, and the problem characterized by large number of parameters, to better search for a global minimum, a Pattern Search method has been preferred to a Newton-like method. The optimization was divided in two different parts:

- A three-parameter optimization, where only the Q, R diagonals were considered. In this case, thanks to the low number of parameters, an extended Pattern Search with discrete derivatives (Gradient and Hessian, calculated using a small sampling cubical crown of 27 sampling points) has been used. The results were used as a base for the second optimization cycle.
- A thirteen-parameter optimization, where the terms from R, S and Q matrices strongly linked to the firsts off -plane bending modes are considered. In this case a classical Pattern Search (derivative free) was used. In the process, the three parameter matrices are

multiplied by a different dilatation constant each and this, coupled with a variable step progression, seems to help the search for global minimum rather than local ones.

The main method constraints are the following:

- Control surfaces (Aileron, Gust LC Tab, elevators) maximum angular speed of 100 deg/s, to implicitly reduce the maximum actuator frequency and torque required.
- Maximum aileron deflection of ±10 deg, maximum Gust LC-Tab deflection of ±20 deg, maximum elevator deflection of ±15 deg. (In practice, the maximum control surface deflection reached will be about ±5 deg., at least in the range of analysed conditions).

For each iteration, 10 different EAS (1-cosine) gusts (only vertical gusts UP) are considered. The following equations show the Gradient (23) and Hessian matrices (24, 25) used for the first stage of the optimization, for a progression p.

$$D_i = \frac{J(x_i + p) - J(x_i - p)}{2p} \tag{23}$$

$$H_{ii} = \frac{J(x_i + p) + J(x_i - p) - 2J(x_i)}{p^2} \tag{24}$$

$$H_{ij} = \frac{J(x_i + p, x_j + p) - J(x_i + p, x_j - p) - J(x_i - p, x_j + p) + J(x_i - p, x_j - p)}{4p^2} \quad i \neq j \tag{25}$$

4.2.2 Linear Quadratic Estimator (LQE) : Modelling And Optimization

In the LQE design phase, a reduced-order model as close as possible to the physical one had been chosen. This is particularly important because even the less important modes, such as the in-plane bending ones, or some unsteady aerodynamic states, could lead to instability if not properly observed (the perfect observation of such modes is difficult but even detecting the growth of one of them is sufficient).

As far as the mathematical structure of the observer is concerned, it could be described as an optimally tuned Kalman filter (26):

$$\dot{\hat{x}} = (A_r - LC_r)\hat{x} + B_{u_r}u + Ly \tag{26}$$

$$A_r P + P A_r^T - P C_r^T R^{-1} C_r P + Q = 0 \tag{27}$$

$$L = P C_r^T R^{-1} \tag{28}$$

From the equations above, it could be seen that the L matrix (20, 28) is derived from the Riccati algebraic equation (27), in a similar way of the LQR ‘classical’ optimal gain matrix.

To optimize the problem searching for a possible global maximum, a Pattern Search derivative-free approach has been used, differently from the LQR optimization, the chosen cost function is an integral quadratic norm of the error between the physical system and the reduced LQE system. This choice was made for two reasons: better capturing the physical and energetic content of each mode (for a more robust observation) making the optimization procedure smoother and faster (the optimization parameters are in base-10 logarithmic scale). To obtain even more robust results, the procedure has been conducted considering a sinusoidal control surface deflection for every

iteration. In the equation below (29) the cost function can be written as composed by the error vector (e) and a Weight matrix W.

$$J = \int_0^t e^T W e \, dt \tag{29}$$

5 AEROELASTIC VIRTUAL SIMULATOR

This chapter presents the Aeroelastic Virtual Simulator developed for the UERA aircraft configuration. The simulator represents a high-fidelity numerical environment conceived to analyze the aeroelastic behavior of the aircraft and to support the design and assessment of active control strategies, with particular emphasis on Gust Load Alleviation (GLA).

The state–space model of the UERA aircraft, derived and discussed in the previous sections, constitutes the core of the simulator. This model captures the coupled rigid-body and flexible dynamics of the aircraft, including unsteady aerodynamic effects, and is formulated in a form suitable for control design and time-domain simulation. The complete model has been implemented within a Simulink® environment, enabling modularity, extensibility, and straightforward integration of control laws and sensor models. The higher-level block-diagram implementation of the Aeroelastic Simulator is shown in Figure 7, for SOF controller.

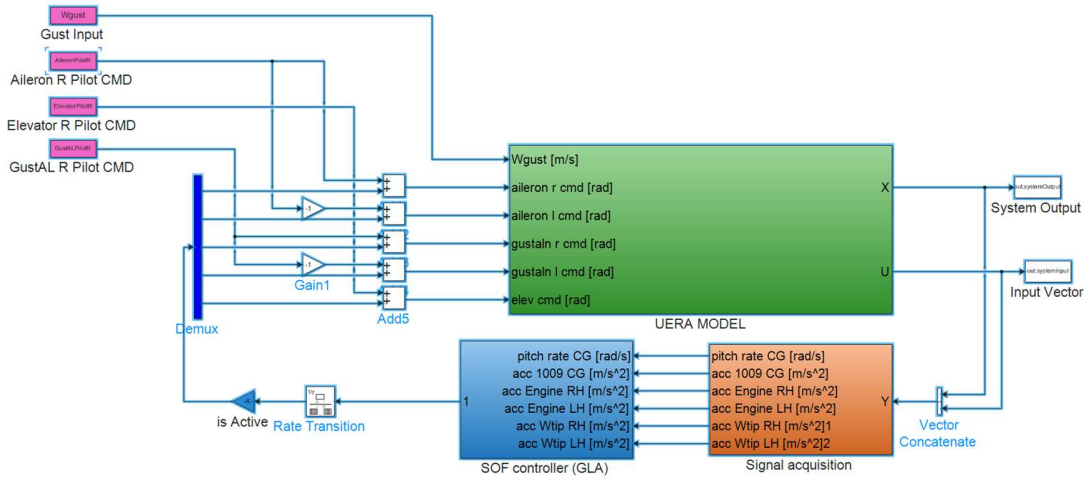


Figure 7: Main view of the developed GLA controller (SOF) implemented aeroelastic virtual simulator

The Simulink project is organized into a set of interconnected functional blocks, each representing a specific subsystem of the aeroelastic simulation framework. This modular structure facilitates both the understanding of the overall architecture and the independent development or modification of individual components. The main blocks composing the simulator are listed below and are discussed in detail in the remainder of this chapter:

- **UERA Model Block**: This block contains the state–space representation of the UERA aircraft aeroelastic model. In addition to the aircraft dynamics, it includes the actuator dynamics associated with the control surfaces used for both flight control and load

alleviation purposes. The block receives control commands as inputs and provides the relevant aircraft states and outputs required for feedback and performance evaluation.

- **Acquisition Block**: The acquisition block models the onboard sensor system used to measure the quantities employed as feedback signals by the controller. It includes the selection and placement of sensors (e.g., accelerometers, rate gyros, or strain-related measurements), as well as their dynamic behavior. This block allows the simulation of realistic measurement signals and provides a coherent interface between the physical aircraft model and the control system.

- **Controller Block:** The controller block implements the active control logic within the Simulink environment. It provides a general framework for the integration of Gust Load Alleviation control laws. As an illustrative example, a Static Output Feedback (SOF) controller is presented and implemented. This block processes the measured outputs from the acquisition system and generates the corresponding control surface commands, which are then applied to the UERA model through the actuator dynamics. The SOF block can be replaced by whichever control scheme developed, like the LQG.

The described architecture enables closed loop aeroelastic simulations under various flight and disturbance conditions, such as discrete or continuous gust encounters. As a result, the Aeroelastic Virtual Simulator represents a powerful tool for evaluating the effectiveness of GLA strategies and for supporting the development of advanced control concepts for the UERA aircraft configuration.

The controller frequency is 1000Hz, equivalent to 0.001s of sampling time. The dynamic of the sensors is modelled as well, considering sensor accuracy, signal discrete-time filtering to remove high frequency noise, rate and transmission delays, discrete numerical integrators.

Many output are available, since the whole state vector is saved it is possible to reconstruct whichever system output.

Default outputs of the Simulink are the bending and torsional moment at the Wing Load Monitoring Station (WS01 to WS05) and the acceleration at the center of gravity, engine and wing tip of the right wing. Since the gust and the controller are symmetric, only the right-hand side of the aircraft is plotted.

Additional simulation results are plotted, like the control surface commands and deflections.

All the results are presented both for the OL and CL cases

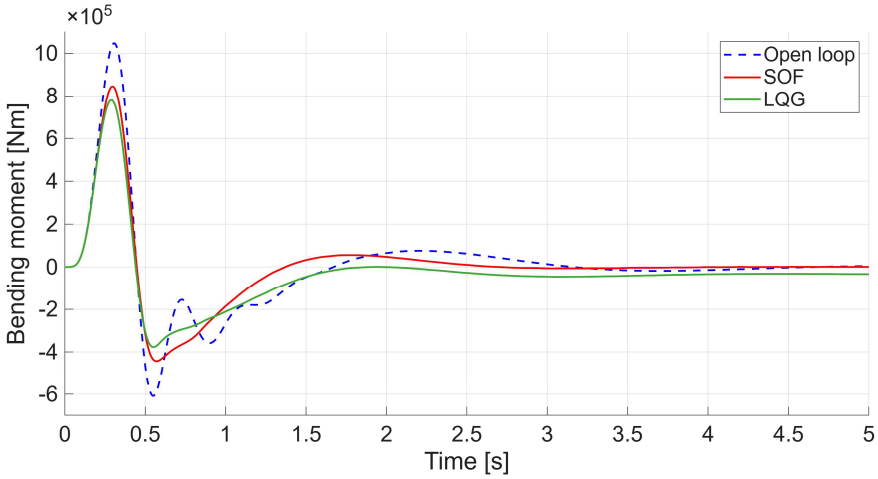


Figure 8: WS01 out of plane bending moment: comparison between open loop, SOF and LQG controllers

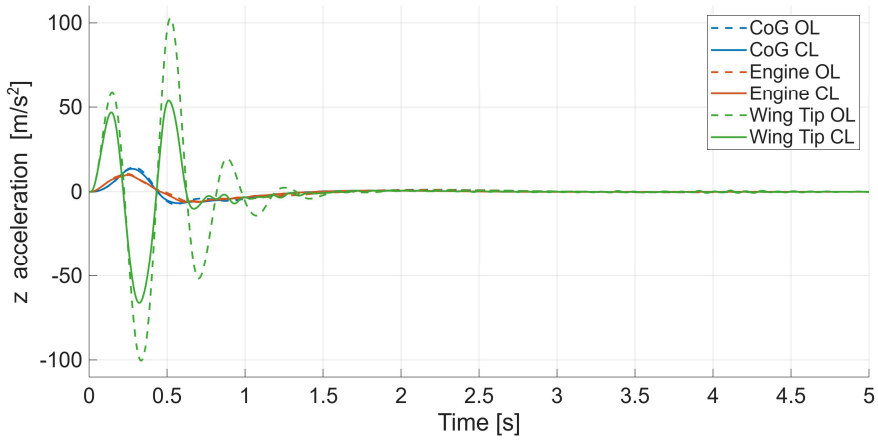


Figure 9: Accelerations at different locations for SOF controller

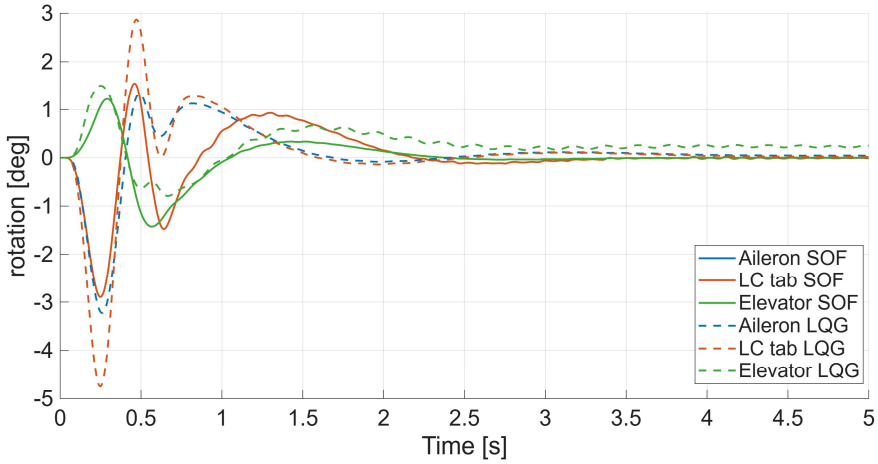


Figure 10: Control surface deflection for SOF and LQG controllers

The gust input is defined as prescribed by EASA/CS 25.341 paragraph [6].

$$v_g = \begin{cases} \frac{U_g}{2}\left(1 - \cos\left(\frac{\pi x}{H}\right)\right) & 0 < x < 2H \\ 0 & x > 2H \end{cases} \tag{30}$$

where x is the distance of penetration in the gust.

H is the gust gradient and U_g *Design gust velocity*, expressed in Equivalent Airspeed (EAS), and is given by the following formula:

$$U_g = U_{ref} F_g \left(\frac{H}{350}\right)^{\frac{1}{6}} \tag{31}$$

Where:

- U_g is the *Reference gust velocity*, defined as a function of altitude and flight condition.
- U_{ref} reduction of gust intensity along the flight profile.
- *H Gust gradient is* the distance along the flight path over which the gust reaches its peak velocity.
- $\left(\frac{H}{350}\right)^{\frac{1}{6}}$ is the scaling factor that adjusts the gust intensity based on the gust gradient; 350 (ft) is the reference gradient defined in CS-25 [6].

Parameter Uref varies with the altitude with law:

$$Uref = \begin{cases} 17.07\ {}^{m}/_{s} - \frac{(17.07\ {}^{m}/_{s} - 13.42\ {}^{m}/_{s})}{4572\ m}\, h & 0 < h < 4572\ m \\ 13.41\ {}^{m}/_{s} - \frac{(13.41\ {}^{m}/_{s} - 6.25\ {}^{m}/_{s})}{(18880\ m - 4572\ m)}\,(h - 4572\ m) & 4572\ m < h < 18880\ m \end{cases} \tag{32}$$

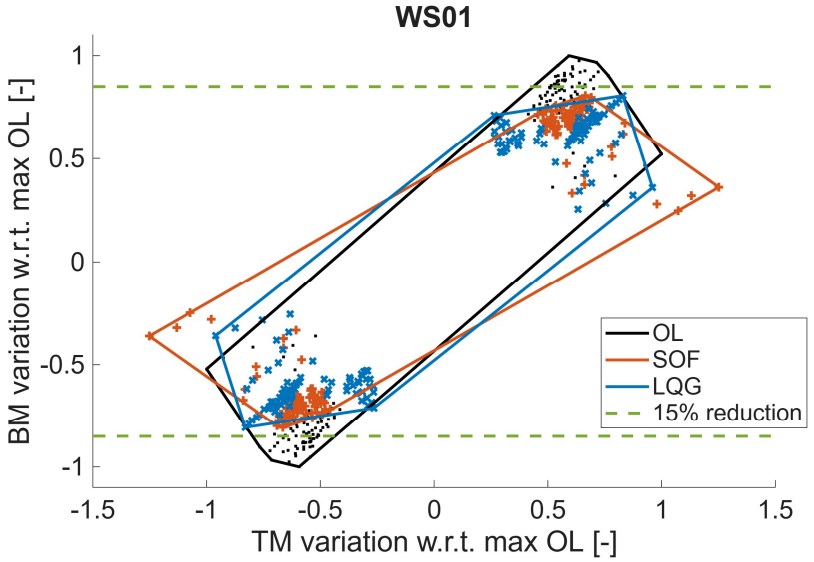


Figure 11 – Comparison of the WS01 bending/torque envelope between open loop (OL), SOF and LQG controller

Gust loads alleviation (GLA) systems closed loop resulting performances, in terms on wing root bending moment reduction with respect to open loop gust impulse, are showed in Figure 11 where

2D loads envelope at Wing Root (WS01) section are plotted against the project HERWINGT [1] compliance loads alleviation requirement = - 15 %(green line) wing root bending moment. A part bending moment, to be highlighted the better performance of LQG, with respect to SOF, in reducing wing torsion increases since torque is considered into the LQR cost function.

In following Table 3 shows maximum WRBM reduction for this work, satisfying the GLA requirement.

Controller	WRBM reduction
SOF	-19.4%
LQG	-22.6%

Table 3 – GLA controllers WRBM maximum reduction wrt OL condition

6 CONCLUSIONS

This work has presented a comprehensive numerical framework for the assessment of active load alleviation technologies applied to a high–aspect-ratio regional aircraft wing representative of the UERA AR16 configuration. The integration of a reduced-order aeroelastic state-space model, derived from a NeoCASS-based structural and aerodynamic formulation, with a modular Simulink-driven aero-servo-elastic simulator has enabled the systematic design and evaluation of both gust and manoeuvre load alleviation strategies. Numerical analyses have demonstrated that active control solutions can achieve significant reductions in critical load metrics, with wing root bending moment decreases on the order of 20% under discrete gust excitation in closed-loop conditions using GLA controllers, relative to the open-loop baseline. A simple proportional MLA controller highlights too the importance of aerodynamic load distribution during sustained maneuvers, achieving a 20% reduction in WRBM too. Future studies will incorporate aerodynamic stall effects, actuator force saturation, and additional morphing devices to further improve and optimize this capability.

Overall, the study highlights the fundamental role of active load control in enabling lightweight, high-efficiency wing designs by mitigating the aeroelastic penalties associated with increased flexibility.

The developed GLA controllers will be tested on a 1:6 iso-frequency scaled wind tunnel model, to assess both controller effectiveness and achieve TRL5 by the end of the HERWINGT project [1].

ACKNOWLEDGEMENTS

This study is part of the Hybrid Electric Regional Wing Integration Novel Green Technologies (HERWINGT) project. This project has received funding from the Clean Aviation Joint Undertaking under the European Union's Horizon Europe research and innovation program under grant agreement ID 101102010. Views and opinions expressed are however those of the authors only and do not necessarily reflect those of the European Union or the Clean Aviation Joint Undertaking. Neither the European Union nor the granting authority can be held responsible for them.

REFERENCES

[1] "HERWINGT: Hybrid Electric Regional Wing Integration Novel Green Technologies," [Online]. Available: https://herwingt-project.eu/home

[2] "HERA: Hybrid Electric Regional Architecture," [Online]. Available: https://project-hera.eu/home

[3] L. Cavagna, S. Ricci, and L. Travaglini, "NeoCASS: An Integrated Tool for Structural Sizing, Aeroelastic Analysis and MDO at Conceptual Design Level," Progress in Aerospace Sciences, vol. 47, no. 8, pp. 621–635, 2011.

[4] L. Cavagna, S. Ricci, and L. Riccobene, "Structural Sizing, Aeroelastic Analysis, and Optimization in Aircraft Conceptual Design, "Journal of Aircraft, vol. 48, no. 6, pp. 1840–1855, 2011.

[5] L. Cavagna, S. Ricci, and L. Travaglini,"Aeroelastic Analysis and Optimization at Conceptual Design Level Using NeoCASS Suite,"in Proc. AIAA/ASME/ASCE/AHS/ASC Structures, Structural Dynamics and Materials Conference, 2011.

[6] EASA CS 25 Large Aeroplanes [Online]. Available: https://www.easa.europa.eu/en/document-library/certification-specifications/cs-25-amendment-28, Chapt: 25.302, 25.341, 25.629, 25.671, 25.1309, 2025,

[7] F. Fonte, S. Ricci, and P. Mantegazza, "Gust load alleviation for a regional aircraft through a static output feedback,"Journal of Aircraft, vol. 52, no. 5, pp. 1559–1574, 2015.

[8] S. Ricci, N. Paletta, S. Defoort, E. Benard, J. E. Cooper, and P. Barabinot, "U-HARWARD: A CS2 EU Funded Project Aiming at the Design of Ultra High Aspect Ratio Wings Aircraft," in Proc. AIAA SciTech Forum, 2022, Paper 0168.

[9] Syrmos, V. L., Abdallah, C. T., Dorato, P., & Grigoriadis, K. (1997). Static Output Feedback - A Survey. *Automatica*, *33*(2). https://doi.org/10.1016/S0005-1098(96)00141-0

[10] Fonte, F., Ricci, S., & Mantegazza, P. (2015). Gust Load Alleviation for a Regional Aircraft Through a Static Output Feedback. *Journal of Aircraft*, *52*(5). https://doi.org/10.2514/1.C032995

COPYRIGHT STATEMENT

The authors confirm that they, and/or their company or organization, hold copyright on all of the original material included in this paper. The authors also confirm that they have obtained permission from the copyright holder of any third-party material included in this paper to publish it as part of their paper. The authors confirm that they give permission, or have obtained permission, from the copyright holder of this paper, for the publication and public distribution of this paper as part of the IFASD 2026 proceedings or as individual off-prints from the proceed